SCIENCE CHINA
Chemistry

• ARTICLES •

March 2016 Vol.59 No.3: 332–337
doi: 10.1007/s11426-015-5492-9

Platinum nanoparticles supported MoS_2 nanosheet for simultaneous detection of dopamine and uric acid

Jie Chao[1], Xiaoyan Han[1], Haofan Sun[1], Shao Su[1*], Lixing Weng[2*] & Lianhui Wang[1]

[1]*Key Laboratory for Organic Electronics & Information Displays; Institute of Advanced Materials, National Syngerstic Innovation Center for Advanced Materials, Nanjing University of Posts & Telecommunications, Nanjing 210023, China*
[2]*College of Geography and Biological Information, Nanjing University of Posts & Telecommunications, Nanjing 210023, China*

Received June 23, 2015; accepted July 27, 2015; published online October 15, 2015

Herein, platinum nanoparticles-decorated molybdenum disulfide (PtNPs@MoS_2) nanocomposite has been synthesized via a microwave-assisted hydrothermal method, which was characterized by transmission electron microscopy (TEM) and powder X-ray diffraction (XRD). This MoS_2-based nanocomposite modified glass carbon electrode (PtNPs@MoS_2/GCE) exhibited excellent electrocatalytic activity toward dopamine (DA) and uric acid (UA) due to their synergistic effect. Two well-defined oxidation peaks of DA and UA were obtained at PtNPs@MoS_2/GCE with a large peak separation of 160 mV (DA-UA), suggesting that the modified electrode could individually or simultaneously analyze DA and AA. Under the optimal conditions, the peak currents of DA and UA were linearly dependent on their concentrations in the range of 0.5–150 and 5–1000 μmol/L with detection limit of 0.17 and 0.98 μmol/L, respectively. The proposed MoS_2-based sensor can also be employed to examine DA and UA in real samples with satisfactory results. Therefore, the PtNPs@MoS_2 nanocomposite might offer a good possibility for electrochemical sensing and other electrocatalytic applications.

molybdenum disulfide, platinum nanoparticles, dopamine, uric acid

Citation: Chao J, Han XY, Sun HF, Su S, Weng LX, Wang LH. Platinum nanoparticles supported MoS_2 nanosheet for simultaneous detection of dopamine and uric acid. *Sci China Chem*, 2016, 59: 332−337, doi: 10.1007/s11426-015-5492-9

1 Introduction

Dopamine (DA) and uric acid (UA) always coexist in real biological samples, which are considered as crucial small biomolecules for physiological processes in human metabolism. Abnormal DA or UA concentrations lead to several diseases, such as schizophrenia, Parkinson's disease, hyperglycemia and Lesch-Nyhan syndrome [1–3]. Therefore, considering their importance in analytical and diagnostic application, DA and UA detection with high sensitivity and selectivity gradually attracted many scientists' attention [4]. Unfortunately, it is hard to distinguish DA and UA at conventional solid electrode due to their overlapping oxidation peaks [5–7]. To solve the problem, many materials have been employed to prepare modified electrodes, such as poly(3-(3-pyridyl) acrylic acid) [8], platinum nanoparticles [9], graphene [10], silicon nanowires [11] and other nanomaterials [12], which could selectively determine DA and UA.

Like graphene, molybdenum disulfide (MoS_2) is a typical layered nanomaterial, which could be easily exfoliated to few layers even single layer nanosheet [13–16]. Up to now, MoS_2 nanosheet has been successfully employed in catalysis [17], lithium batteries [18], capacitors [19], and biological/chemical sensors [20–22] due to its ultrathin structure and unique properties. Taking the sensor for example, Zhang's group [22] utilized MoS_2 nanosheet as a sensing platform to detect DNA and small molecules. Yang and co-workers

*Corresponding authors (email: iamssu@njupt.edu.cn; lxweng@njupt.edu.cn)

[23] constructed a label-free and ultrasensitive electrochemical DNA biosensor based on thin-layer MoS_2. To improve the performances of MoS_2-based sensors, noble metal nanoparticles have been introduced on the surface of MoS_2 nanosheets [24]. Such noble metal nanoparticles-decorated MoS_2 nanocomposite possesses the specific feature of both noble metal nanoparticles and MoS_2. Yuwen *et al*. [25] reported palladium nanoparticles (PdNPs)-decorated MoS_2 have greatly enhanced catalytic activity compared to a commercial Pd/C catalyst. Our group had already used gold nanoparticles (AuNPs) supported MoS_2 nanocomposite to construct sensors for DA [26], glucose [27] and Rhodamine 6G [28] determination.

In this work, PtNPs-decorated MoS_2 hybrid nanomaterial was prepared by a microwave-assisted hydrothermal method. The electrochemical behavior of the PtNPs@MoS_2 modified electrode was characterized by cyclic voltammetry (CV) and differential pulse voltammetry (DPV). The PtNPs@MoS_2 nanocomposite film modified electrode exhibited excellent electrocatalytic activity toward DA and UA. The oxidation peaks of DA and UA were 0.20 and 0.36 V at PtNPs@MoS_2 modified electrode, respectively, which permitted individually or simultaneously detecting DA and UA in buffer and in real samples.

2 Experimental

2.1 Chemicals and reagents

Potassium hexacyanoferrate (III) ($K_3Fe(CN)_6$, ⩾99.5%), sodium dihydrogen phosphate ($NaH_2PO_4\cdot 2H_2O$, ⩾99.0%), and disodium hydrogen phosphate (Na_2HPO_4, ⩾99.0%) were purchased from Sinopharm Chemical Reagent Co., Ltd. (China). Molybdenum (IV) sulfide powder (<2 mm, 99%), hydrogen hexachloroplatinate (IV) ($H_2PtCl_6\cdot xH_2O$, ⩾99.9%), uric acid (UA), dopamine (DA) were purchased from Sigma-Aldrich (USA). The ultrapure water from Millipore system (>18 MΩ cm) was employed to prepare all aqueous solutions.

2.2 Apparatus and measurements

Electrochemical performances of different modified electrodes were tested with an Autolab PGSTAT302 (Metrohm China Ltd., Switzerland). The electrochemical measurements were achieved in 0.1 mol/L phosphate buffer (PB, pH 7.0) by a standard three-electrode system. Different modified electrodes, a platinum wire and a saturated calomel electrode (SCE) were used as the working electrodes, counter and the reference electrode, respectively. The transmission electron microscopy (TEM) images were recorded using Philips CM 200 electron microscope (Holland) operated at 200 kV. Surface morphologies of MoS_2 nanosheet were examined with atomic force microscope (AFM, Bruker, Germany). Powder X-ray diffraction (XRD) was performed to characterize PtNPs@ MoS_2 nanocomposite by using a D/max-γB diffractometer.

2.3 Preparation of MoS_2 nanosheet and PtNPs@MoS_2 nanocomposite

MoS_2 nanosheet was prepared according to our previous work [28,29]. The exfoliated few layers MoS_2 nanosheet was purified three times and further used to synthesize PtNPs@MoS_2 nanocomposite.

The PtNPs@MoS_2 nanocomposite was prepared similar to our previous work [26]. Typically, 100 μL (50 mmol/L) CMC, 50 μL (100 mmol/L) $NaBH_4$ and 300 μL (5 mmol/L) H_2PtCl_6 were successively added into 10 mL (10 μg/mL) MoS_2 nanosheets solution. After that the reaction mixture was heated to 100 °C for 5 min in the microwave reactor. Finally, the product of PtNPs@MoS_2 was centrifugated at least twice for the purification.

2.4 Preparation of PtNPs@MoS_2/GCE

Briefly, 5 μL of as-prepared PtNPs@MoS_2 nanocomposite was dropped on the cleaned glassy carbon electrode (GCE) and dried at room temperature. The modified electrode was called PtNPs@MoS_2/GCE. For comparison, MoS_2/GCE was prepared by a similar procedure.

3 Results and discussion

3.1 Characterization of MoS_2 and PtNPs@MoS_2

As shown in Figure 1(a), TEM image displayed the exfoliated MoS_2 nanosheets had a typical layered nanostructure (Figure 1(a)). In order to determine the thickness of the MoS_2 nanosheet, atomic force microscope (AFM) was employed to characterize it. The average height of MoS_2 nanosheet was about 1.08 nm, suggesting that the exfoliated MoS_2 nanosheet was single layer (Figure 1(c)) [30,31]. After decorating, 5 nm PtNPs dispersed homogeneously onto the surface of MoS_2 nanosheet, indicating that PtNPs@ MoS_2 nanocomposite was successfully synthesized (Figure 1(b)). We also utilized X-ray diffraction (XRD) to confirm the structure of the PtNPs@MoS_2 nanocomposite. As shown in Figure 1(d), four strong diffraction peaks emerged at 39.8°, 46.4°, 68.3°, and 81.8° after PtNPs supported on the surface of MoS_2 nanosheet, which can be assigned to the planes of Pt crystal (JCPDS No. 87-0642) [25,32,33]. All the results indicated the successful formation of PtNPs@ MoS_2 nanocomposite.

3.2 Electrochemical characterization of PtNPs@MoS_2/GCE

The electrochemical performances of different modified

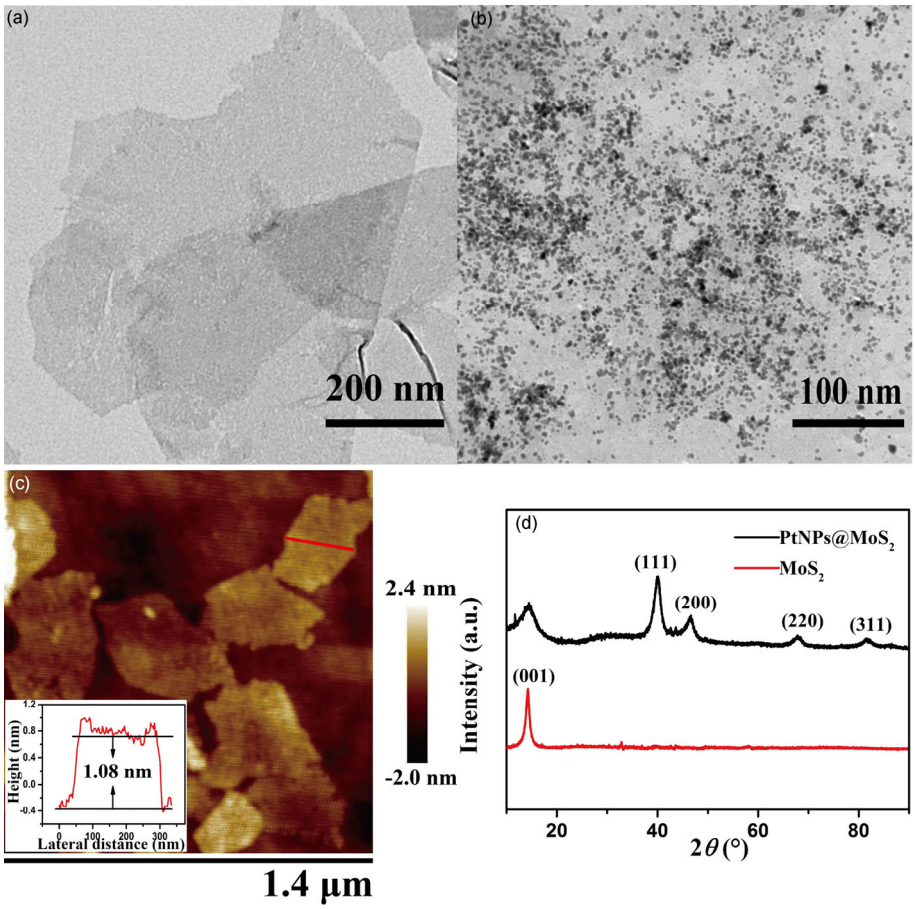

Figure 1 TEM images of the MoS_2 nanosheet (a) and PtNPs@MoS_2 nanocomposite (b); (c) AFM image of MoS_2 nanosheet; (d) XRD patterns of MoS_2 nanosheet and PtNPs@MoS_2 nanocomposite.

electrodes were evaluated by cyclic voltammetry (CV) in 0.1 mol/L PB (pH 7.0) containing 5 mmol/L $[Fe(CN)_6]^{3-/4-}$. Figure 2(A) shows both anodic and cathodic peak currents of PtNPs@MoS_2/GCE (curve c) and MoS_2/GCE (curve b) were larger than that of the bare GCE (curve a), suggesting that these modified electrodes have better electrochemical performances. As we know, MoS_2 possessed high surface-to-volume ratio and PtNPs had excellent electrical conductivity, enabling PtNPs@MoS_2 nanocomposite to efficiently facilitate the electron transfer between the redox probe and the electrode surface. This better electrochemical performance could be attributed to the synergistic effect of PtNPs and MoS_2. In addition, the redox peak currents of PtNPs@MoS_2/GCE were 10.3 and 2.9 times higher than those of bare GCE and MoS_2/GCE, respectively, suggesting that PtNPs@MoS_2 nanocomposite has prominent electrocatalytic activity. The capacity of electron transfer of different electrodes was also investigated by electrochemical impedance spectroscopy (EIS). EIS results also proved that PtNPs@MoS_2/GCE had better conductivity than pure MoS_2. As shown in Figure 2(B), the electron transfer resistance (Rct) of the MoS_2/GCE (curve b) was obviously increased due to its poor conductivity, which was much larger than that of the bare GCE (curve a) [26]. Meanwhile, the Rct of PtNPs@MoS_2/GCE decreased greatly, suggesting the PtNPs@MoS_2 nanocomposite efficiently improved the conductivity and facilitated the electron transfer process (curve c). All the results indicated that PtNPs@MoS_2 nanocomposite might be a potential nanomaterial for electrochemical sensing application.

3.3 Voltammetric oxidation of dopamine and uric acid at different electrodes

The electrochemical oxidation behavior of DA and UA at bare GCE, MoS_2/GCE and PtNPs@MoS_2/GCE was studied. Unfortunately, a broad oxidation peak at 0.45 V was obtained at bare GCE (Figure 3, curve a), indicating that the bare GCE cannot distinguish DA and UA. Interestingly, two well-defined oxidation peaks were obtained at MoS_2/GCE, located at 0.20 and 0.36 V, respectively (Figure 3, curve b). However, these peak currents were not large enough to determine DA and UA with high sensitivity due to the poor conductivity of MoS_2. In order to obtain better detection performances, PtNPs@MoS_2/GCE was used to determine DA and UA. As expected, two larger oxidation peaks were

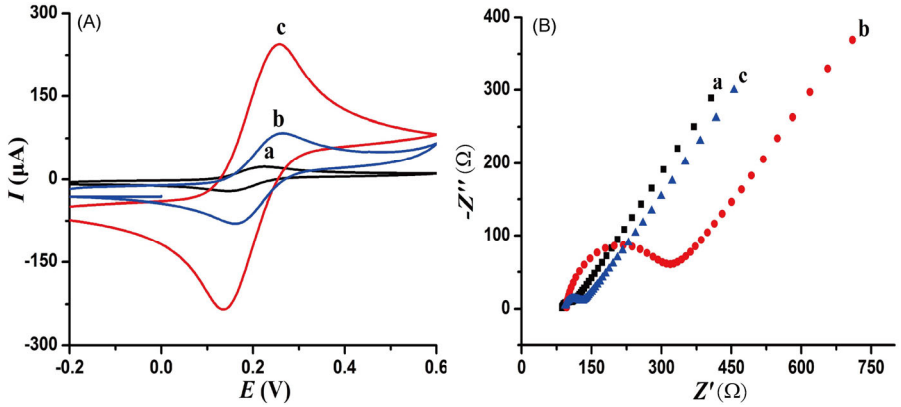

Figure 2 (A) Cyclic voltammograms of GCE (a), MoS_2/GCE (b) and PtNPs@MoS_2/GCE (c) in 0.1 mol/L (pH 7.0) PB containing 5 mmol/L $Fe(CN)_6^{3-/4-}$. Scan rate: 100 mV/s. (B) Nyquist plots of GCE (a), MoS_2/GCE (b) and PtNPs@MoS_2/GCE (c) in 0.1 mol/L PB containing 5 mmol/L $Fe(CN)_6^{3-/4-}$.

obtained at PtNPs@MoS_2/GCE (Figure 3, curve c). The peak currents of DA and UA at PtNPs@MoS_2/GCE were about 2.7 and 1.7 times larger than those at MoS_2/GCE, respectively, indicating that the synergistic effect of PtNPs@MoS_2 made the electrochemical performances better than pure MoS_2. The large peak current and enough peak separation (160 mV) of DA and UA permitted the PtNPs@MoS_2/GCE to sensitively and selectively determine DA and UA.

3.4 Effect of scan rate and pH value on the electrochemical response of DA and UA

The effect of scan rate on the CV responses of DA and UA at PtNPs@MoS_2/GCE were investigated. As shown in Figure S1 (Supporting Information online), the peak currents of DA and UA linearly increased with the square root of the scan rate in the range of 10–300 mV/s, indicating that the electrochemical reaction is a typical diffusion-controlled electrochemical process [34]. Figure S2 shows the influence of pH value on the peak potentials of DA and UA at PtNPs@MoS_2/GCE. The $E^{0\prime}$ (the formal potential) of DA and UA was found to be linearly proportional to the solution pH value in the range of 5.5–7.5 with a slope of –62.4 and –41.5 mV/pH, respectively. Moreover, the peak currents of DA and UA increased with the increasing pH value, and reached a maximum value when the pH equaled 7.0. Because pH 7.0 was close to the physiological pH environment, it was selected as optimal condition for the DA and UA determination.

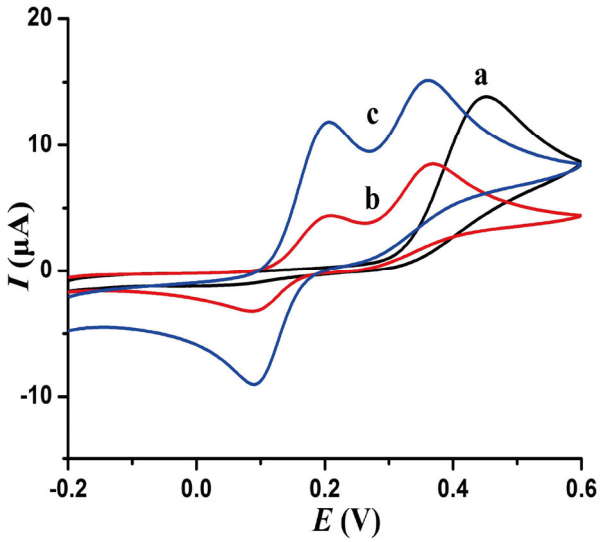

Figure 3 Cyclic voltammograms of bare GCE (a), MoS_2/GCE (b) and PtNPs@MoS_2/GCE (c) in 0.1 mol/L PB (pH 7.0) containing of 300 μmol/L DA and 1 mmol/L UA. Scan rate: 100 mV/s.

3.5 Individual and simultaneous determination of DA and UA

At first, individually determining DA and UA at PtNPs@MoS_2/GCE was investigated by different pulse voltammetric (DPV) techniques. As shown in Figure S3, the oxidation peak currents of DA and UA were linear with the concentration from 0.5 to 200 μmol/L (Figure S3(a, b)) and 5 to 2000 μmol/L (Figure S3(c, d)), respectively. The detection limit of DA and UA was 0.11 and 0.12 μmol/L (S/N=3), respectively.

On the basis of the above results, PtNPs@MoS_2/GCE was employed to selectively determine DA and UA due to the large peak separation of them. Generally, DA concentration was increasing while the concentration of UA kept constant. As shown in Figure 4(a, b), the electrochemical responses of DA was linear with the increasing DA concentration in the range from 0.5 to 150 μmol/L with detection limit of 0.12 μmol/L. More importantly, there was almost no significant influence on the electrochemical performances of UA with the changes of DA concentration. Similarly, the oxidation peak currents of UA (Figure 4(c, d)) were linear with the increasing concentration in the range from 5 to 1000 μmol/L with detection limit of 0.8 μmol/L (S/N=3).

Furthermore, the feasibility of simultaneous determina-

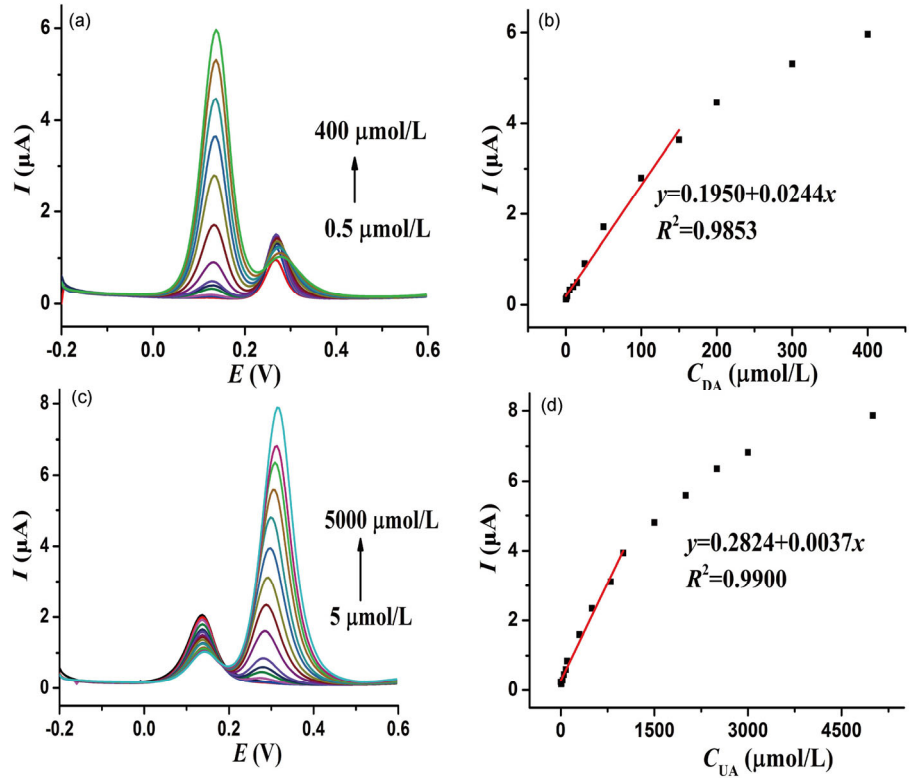

Figure 4 (a) DPV curves of the PtNPs@MoS_2/GCE in 0.1 mol/L PB solution (pH 7.0) containing 100 μmol/L UA and different concentrations of DA from 0. 5 to 400 μmol/L; (b) calibration curve of DA concentration versus the anodic peak currents; (c) DPV curves of the PtNPs@MoS_2/GCE in 0.1 mol/L PB solution containing 100 μmol/L DA and different concentrations of UA; (d) calibration curve of UA concentration versus the anodic peak currents.

tion of DA and UA was also studied at PtNPs@MoS_2/GCE. As shown in Figure 5, both the electrochemical responses of DA and UA increased with their concentrations simultaneously increasing. The peak currents of DA and UA were linear with the concentrations in the ranges of 0.5–150 μmol/L for DA and 5–1000 μmol/L for UA with detection limit of 0.17 and 0.98 μmol/L (S/N=3), respectively. All results proved that the proposed MoS_2-based sensor could well separate and determine the DA and UA when they coexist in buffer solution. The electrochemical performances of the MoS_2-based sensor (linear range and detection limit) were comparable to or better than the results reported for simultaneous determination of DA and UA at other nanomaterials-based electrodes [35,36] (Table S1, Supporting Information online).

3.6 Real sample analysis

In order to verify the practical performance of the proposed method for detection of DA and UA in real samples, PtNPs@MoS_2/GCE was employed to detect DA and UA in 1% human serum. The obtained results are displayed in Table 1. The excellent recovery (>99%) and small relative standard deviation (<4%) showed that the fabricated sensor could be used to determine DA and UA in real samples.

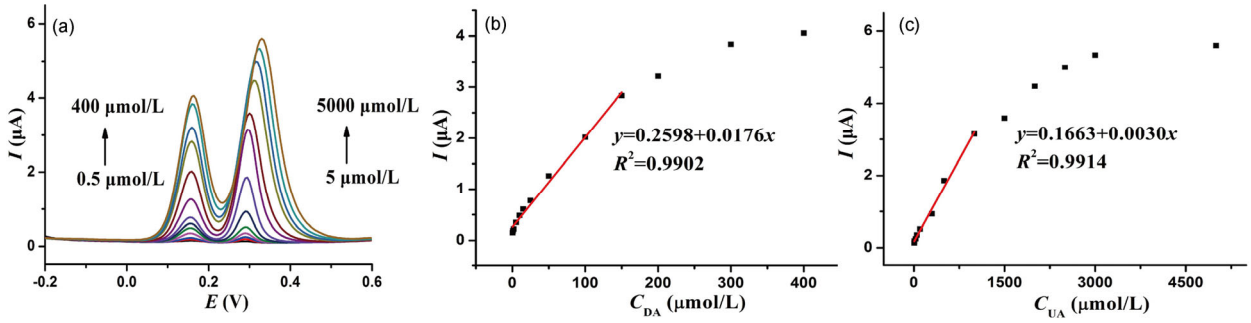

Figure 5 (a) DPV curves of the PtNPs@MoS_2/GCE in 0.1 mol/L PB solution (pH 7.0) containing different concentrations of DA and UA. The concentrations in the range from 0.5 to 400 μmol/L for DA and 5 to 5000 μmol/L for UA, respectively (from bottom to up). (b) Calibration curve of DA concentration versus the anodic peak currents. (c) Calibration curve of UA concentration versus the anodic peak currents.

Table 1 Determination of DA and UA in human serum samples (n=3)

Sample	Add (μmol/L)		Found (μmol/L)		Recovery (%)		RSD (%)	
	DA	UA	DA	UA	DA	UA	DA	UA
Serum 1	1	20	0.9983	20.06	99.83	100.32	0.52	2.88
Serum 2	5	50	5.044	50.75	100.88	99.93	2.19	2.83
Serum 3	10	100	9.998	100.09	99.98	100.12	3.44	2.59
Serum 4	15	300	14.99	299.91	99.97	99.97	2.61	3.31

4 Conclusions

In this work, we have successfully fabricated an electrochemical sensor based on PtNPs@MoS_2 nanocomposite. The synergistic effect of PtNPs and MoS_2 efficiently improved electrocatalytic activity towards the oxidation of DA and UA. DA and UA could be easily distinguished at the PtNPs@MoS_2 nanocomposite modified electrode, suggesting the sensor can be employed in the sensitive and selective determination of DA and UA. Additionally, the as-prepared MoS_2-based sensor could be used to determine DA and UA in real samples. All results indicated that the proposed PtNPs@MoS_2 nanocomposite may be a promising candidate nanomaterial for the development of electrochemical sensors.

Acknowledgments This work was supported by the National Basic Research Program of China (2012CB933301), the National Natural Science Foundation of China (21305070, 21475064), the Natural Science Foundation of Jiangsu Province (BK20130861), the Sci-Tech Support Plan of Jiangsu Province (BE2014719), Specialized Research Fund for the Doctoral Program of Higher Education of China (IRT1148, 20133223120013), and the Priority Academic Program Development of Jiangsu Higher Education Institutions.

Conflict of interest The authors declare that they have no conflict of interest.

Supporting information The supporting information is available online at http://chem.scichina.com and http://link.springer.com/journal/11426. The supporting materials are published as submitted, without typesetting or editing. The responsibility for scientific accuracy and content remains entirely with the authors.

1 Noroozifar M, Khorasani-Motlagh M, Akbari R, Parizi MB. *Biosens Bloelectron*, 2011, 28: 56–63
2 Sheng ZH, Zheng XQ, Xu JY, Bao WJ, Wang FB, Xia XH. *Biosens Bioelectron*, 2012, 34: 125–131
3 Sun CL, Lee HH, Yang JM, Wu CC. *Biosens Bioelectron*, 2011, 26: 3450–3455
4 Zhang Y, Xia Z, Liu H, Yang MT, Lin LL, Li QZ. *Sens Actuator B: Chem*, 2013, 188: 496–501
5 Nowall WB, Kuhr WG. *Anal Chem*, 1995, 67: 3583–3588
6 Popa E, Notsu H, Miwa T, Tryk DA, Fujishima A. *Electrochem Solid-State Lett*, 1999, 2: 49–51
7 Weng J, Xue JM, Wang J, Ye JS, Cui HF, Sheu FS, Zhang QQ, Wang J. *Adv Funct Mater*, 2005, 15: 639–647
8 Zhang YZ, Su S, Pan Y, Zhang LP, Cai YJ. *Annali Di Chimica*, 2007, 8: 665–674
9 Xu TQ, Zhang QL, Zheng JN, Lv ZY, Wei J, Wang AJ, Lv ZY, Wei J, Wang AJ, Feng JJ. *Electrochimca Acta*, 2014, 115: 109–115
10 Zhou M, Zhai YM, Dong SJ. *Anal Chem*, 2009, 81: 5603–5613
11 Su S, Wei XP, Guo YY, Zhong YL, Su YY, Huang Q, Fan CH, He Y. *Part Part Syst Charact*, 2013, 30: 326–331
12 Ardakani MM, Talebi A, Naeimi H, Barzoky MN, Taghavinia N. *J Solid State Electrchem*, 2009, 13: 1433–1440
13 Huang X, Zeng ZY, Zhang H. *Chem Soc Rev*, 2013, 42: 1934–1946
14 Li H, Wu J, Yin ZY, Zhang H. *Accounts Chem Res*, 2014, 47: 1067–1075
15 Huang X, Tan CL, Yin ZY, Zhang H. *Adv Mater*, 2014, 26: 2185–2204
16 Zhao J, Zhang Z, Yang S, Zheng H, Li Y. *J Alloy Compd*, 2013, 559: 87–91
17 Tan CL, Zhang H. *Chem Soc Rev*, 2015, 44: 2713–2731
18 Wang JZ, Lu L, Lotya M, Coleman JN, Chou SL, Liu HK, Minett AI, Chen J. *Adv Energy Mater*, 2013, 3: 798–805
19 Zeng ZY, Yin ZY, Huang X, Li H, He QY, Lu G, Zhang H. *Angew Chem Int Ed*, 2011, 50: 11093–11097
20 Chen Y, Tan CL, Zhang H, Wang LZ. *Chem Soc Rev*, 2015, 44: 2681–2701
21 Wu SX, Zeng ZY, He QY, Wang ZJ, Wang SJ, Du YP, Yin ZY, Su XP, Chen W, Zhang H. *Small*, 2012, 8: 2264–2270
22 Zhu C, Zeng Z, Li H, Li F, Fan C, Zhang H. *J Am Chem Soc*, 2013, 135: 5998–6001
23 Wang XX, Nan FX, Zhao JL, Yang T, Ge T, Jiao K. *Biosens Bioelectron*, 2015, 64: 386–391
24 Huang X, Zeng ZY, Bao SY, Wang MF, Qi XY, Fan ZX, Zhang H. *Nat Commun*, 2013, 4: 1444
25 Yuwen LH, Xu F, Xue B, Luo ZM, Zhang Q, Bao BQ, Su S, Weng LX, Huang W, Wang LH. *Nanoscale*, 2014, 6: 5762–5769
26 Su S, Sun HF, Xu F, Yuwen LH, Wang LH. *Electroanalysis*, 2013, 25: 2523–2529
27 Su S, Sun HF, Xu F, Yuwen LH, Fan CH, Wang LH. *Microchim Acta*, 2014, 181: 1497–1503
28 Su S, Zhang C, Yuwen LH, Chao J, Zuo XL, Liu XF, Song CY, Fan CH, Wang LH. *ACS Appl Mater Interf*, 2014, 6: 18735–18741
29 Sun HF, Chao J, Zuo XL, Su S, Liu XF, Yuwen LH, Fan CH, Wang LH. *RSC Adv*, 2014, 4: 27625–27629
30 Radisavljevic B, Radenovic A, Brivio J, Giacometti V, Kis A. *Nat Nanotechnol*, 2011, 6: 147–150
31 Lee C, Yan H, Brus LE, Heinz TF, Hone J, Ryu S. *ACS Nano*, 2010, 4: 2695–2700
32 Rao BG, Matte HR, Rao C. *J Clust Sci*, 2012, 23: 929–937
33 Liu S, Wang JQ, Zeng J, Ou JF, Li ZP, Liu XH, Yang SR. *J Power Sources*, 2010, 195: 4628–4633
34 Ghoreishi SM, Behpour M, Fard MHM. *J Solid State Electrchem*, 2012, 16: 179–189
35 Lin KC, Tsai TH, Chen SM. *Biosens Bioelectron*, 2010, 26: 608–614
36 Yang X, Feng B, He XL, Li FP, Ding YL, Fei JJ. *Microchim Acta*, 2013, 180: 935–956